DOI 10.5162/Ultrasonic2025/P1.10

Study on the Wetting Catalytic Mechanism of Acoustic-Driven Flow in Granular Medias

Xinyu Qi[1] *and Li-Yun Fu*[1,2]
[1]*State Key Laboratory of Deep Oil and Gas, China University of Petroleum (East China), Qingdao, China*
[2]*Laboratory for Marine Mineral Resources, Qingdao Marine Science and Technology Center, Qingdao, China*
lfu@upc.edu.cn

Abstract: Vibration-triggered granular flow phenomena are widespread in nature. However, their influencing factors, triggering mechanisms, and flow characteristics remain incompletely elucidated. This study focuses on the triggering effect of near-static-threshold vibrations on shear instability in granular layers under different wettability conditions. The research reveals that under varying wetting conditions, vibrations with specific amplitudes and frequencies can induce system instability, leading to self-accelerating inertial flow or creep flow in the granular layer.

Keywords: vibration, granular, wettability, self-accelerating inertial flow, creep flow

Introduction

Recent studies indicate that the transition of granular media from a jammed (solid) to a flowing (liquid) state represents a subcritical bifurcation process [1][2][3][4][5]. This dynamic behavior closely resembles the multi-interface solid friction behavior [6]. Based on the rate-and-state constitutive law, commonly referred to as the Dieterich-Rice-Ruina model [7][8], the ratio of shear stress τ to normal stress σ_n, denoted as $\mu = \tau/\sigma_n = F_t/F_n$, exhibits a nonlinear evolution characterized by velocity V or shear rate $\dot{\gamma}$. Engineering and geophysical observations indicate that vibrations can induce fluidization by altering the topological structure of particle contact force chains, yet the underlying physical mechanism remains unresolved. Existing studies primarily characterize vibration intensity through the following dimensionless parameters. The first is the peak acceleration ratio, $\Gamma = a/g = (2\pi f)^2 U_0/g$ (U_0 is the displacement amplitude)[9]. The second is the square of vibration velocity $v_a = (2\pi f)U_0$, which drives nonequilibrium transitions through granular temperature $T_g \sim (1/2)mv_a^2$(m is particle mass)[10]. Additionally, collision-like pressure $p_c \sim (1/2)\rho v_a^2$, describes stress transfer in inertia-dominated regimes ($\dot{\gamma} < \dot{\gamma}_0$)[11][12]. Although extensive experimental and theoretical studies have been devoted to analyzing its influencing factors, experimental research on vibration-triggered granular flow mechanisms under different wettability conditions remains absent.

This study investigates the coupling effects of particle system wettability and vibration parameters. Previous studies have shown that shear lubrication can reduce the local threshold friction at particle contacts[13]. We demonstrate that, depending on the interplay between wettability, vibration amplitude, and driving force, the granular layer can exhibit three states: jammed solid, slow creep flow, and fast inertial flow. Experimental results are analyzed within the framework of velocity-weakening friction models.

Experiments

The experiments employed a high-performance vibration testing system comprising a computer, vibration controller, power amplifier, and shaker, with a frequency range of $2-7000$ Hz, a maximum amplitude of 6.5 mm, and the capability to generate high-precision longitudinal sinusoidal waveforms.The shaker surface was coated with uniform glass beads to ensure controlled friction characteristics at the particle-substrate interface. A fixed-volume sample cell ($40mm*40mm*6mm$) was filled with a specific mass of glass microspheres (1 mm diameter). The pore volume $V_{Pore} = V_{Box} - M/\rho$ was calculated, and water was injected to adjust the pore water saturation $S = V_{water}/V_{Pore}$. The granular layer formed a 6 mm thick uniform layer via gravitational sedimentation. After 5 minutes of rest to eliminate aging effects, the platform tilt angle was adjusted until continuous stable flow occurred, with the angle recorded as the maximum static angle θ_m. For constant particle diameter, θ_m is determined by substrate roughness, granular layer thickness, and water saturation. Longitudinal sinusoidal vibrations ($f = 2000/5000$ Hz, amplitude $0.00005-0.00020$ mm) were applied to study granular layer behavior under initial jammed

DOI 10.5162/Ultrasonic2025/P1.10

conditions ($\theta < \theta_r$).

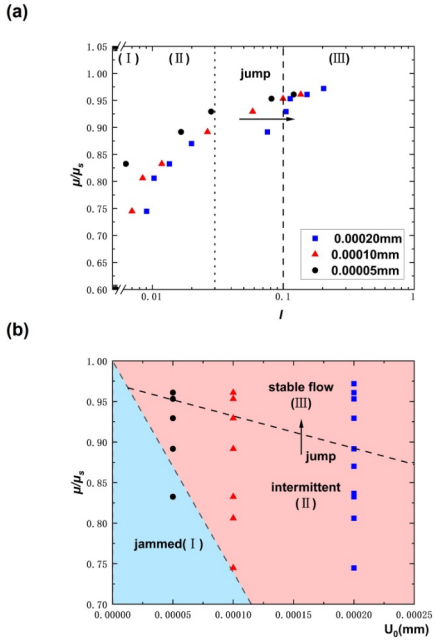

Fig. 1: (a) Evolution of normalized friction coefficient μ/μ_s versus inertial number $I = \dot{\gamma}d\sqrt{\rho/p}$ for a granular layer with thickness $h/d = 6(d = 1\ mm)$ and $f = 2000\ Hz$, under controlled contact roughness. Flow is driven by vibration amplitudes U_0 =0.00005, 0.00010 and 0.00020 mm (black circles, red triangles, and blue squares, respectively). (b) Phase diagram constructed by replotting μ/μ_s from (a) as a function of U_0, illustrating the systems different states.

The vibration amplitude was gradually increased until particle motion was detected, and particle positions were recorded via high-speed imaging. Particle tracking velocimetry (PTV) was used to calculate flow velocity. Fig. 1(a) illustrates the relationship between the normalized friction coefficient ($\mu/\mu_s = tan\theta/tan\theta_m$) and the inertial number $I = \dot{\gamma}d\sqrt{\rho/p}$ (characterizing flow rate)[14] under identical roughness conditions. This curve reflects three dynamic states of the granular layer under vibrational excitation, determined by the systems proximity to the yield threshold (μ/μ_s) and the coupling between vibrational energy and shear stress. In the jammed solid state (Region I), the system is near static yield conditions ($\mu/\mu_s \ll 1$), and the granular layer remains nearly stationary, consistent with the Coulomb jammed state, where weak vibrations fail to destabilize the contact network. In the slow creep flow (Region II), when $\mu/\mu_s \approx 0.9$, the system undergoes a rapid transition from intermittent creep to faster continuous inertial flow near $I \approx 3 \times 10^{-2}$ (Fig. 1(a) dashed line). In the fast inertial flow (Region III), where $I > 10^{-1}$, the flow velocity rivals natural avalanches, driven by inertial stresses and collisional momentum transfer. Here, the system becomes insensitive to vibrational input, indicating that gravity dominates over vibrational forcing near the yield threshold.

Results

Fig. 1(b) constructs a phase diagram of jammed (I), creep (II), and inertial (III) states by replotting μ/μ_s versus amplitude U_0. The non-monotonic transition paths in the $(\mu/\mu_s, U_0)$ plane reveal synergistic coupling between shear stress and vibrational energy: at low μ/μ_s, vibrations dominate flow initiation, with U_0 determining transitions from creep to inertial flow; at high μ/μ_s, shear stress governs dynamics, reducing the critical amplitude U_0. Within the dynamic transition zone (II - III), the inertial number (flow rate) is highly sensitive to U_0 at fixed μ/μ_s. For example, at $\mu/\mu_s = 0.90$, increasing U_0 from 0.00005 mm to 0.00020 mm raises I by approximately 0.06. Fig. 2 systematically quantifies the unlocking threshold $\mu_s{}^*$ of the static granular layer($d = 1\ mm, h = 6\ mm$)as a function of U_0, confirming that vibrational excitation and static shear stress perturbations play complementary roles in triggering.

Discussion

To qualitatively understand the vibration-triggered flow states (Fig. 1), we refer to the heuristic friction model developed by Jaeger et al[15]. In this model, the friction coefficient μ comprises a static component (velocity-weakening term) and a dynamic component (velocity-strengthening term). Vibration-induced shear lubrication reduces μ_s, with pore water saturation SS influencing the system:

$$\mu = \frac{\mu_s(S)}{1 + \alpha_1(S)\widetilde{\dot{\gamma}}^2} + [\beta_0 + \beta_1\eta(S)]\,\widetilde{\dot{\gamma}}^2 \qquad (1)$$

Where, $\mu(\widetilde{\dot{\gamma}})$ is the normalized shear defined above, $\widetilde{\dot{\gamma}} = \dot{\gamma}\sqrt{d/g_\perp}$ (d is the size of the particles) is the dimensionless flow (shear) rate, $\dot{\gamma}$ would scale with V_{flow}/h(h is related to the thickness of the granular layer). $\mu_s(S)$ is the static friction coefficient of particles under different pore water contents, depending on interparticle friction and water content. Pore water content manifests as capillary forces and lubrication effects in the system, regulating the friction coefficient through competition:

$$\mu_s(S) = \mu_{s0}\,[1 + k_1 S(1 - S/S_c) - k_2(S/S_c)^n] \qquad (2)$$

Here, μ_{s0} is the friction coefficient between particles in dry conditions, S is the pore water content, S_c

DOI 10.5162/Ultrasonic2025/P1.10

is the critical pore water content balancing capillary and lubrication effects, k_1 is the capillary force enhancement coefficient related to particle surface hydrophilicity, and k_2 is the lubrication effect parameter controlling the rate of friction coefficient decrease at high water contents.

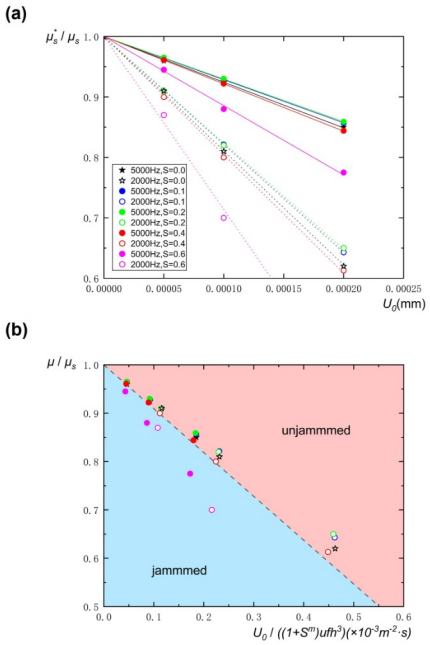

Fig. 2: (a) For a granular layer with thickness $h/d = 6(d = 1\ mm)$, the variation of the normalized static friction coefficient (threshold) μ_s^*/μ_s with vibration amplitude U_0 under different pore water saturations S and vibration frequencies f.Solid symbols correspond to $f = 5000\ Hz$, hollow symbols to $f = 2000\ Hz$. Black, blue, green, red, and pink symbols represent pore water saturations S =0.0, 0.1, 0.2, 0.4 and 0.6, respectively. Lines are fitted using Eq. (3). (b) Data from (a) replotted via Eq. (3), showing the jammed (I) and unjammed (II/III) states of the system, corresponding to the lines in Fig. 1(b).

In Eq.(1) $\alpha_1(S)$ and $\beta_0 + \beta_1\eta(S)$ describe particle geometry and energy loss during collisions, including the coefficient of restitution. $\alpha_1(S)$ and $\beta_1\eta(S)$ describe the contribution of liquids to the velocity-weakening and velocity-strengthening parts, respectively. The black solid line in Fig.3.(a) shows the $\mu(\widetilde{\dot{\gamma}})$ classic curve obtained using Eq.(1) and parameters from reference[15].In this case, spontaneous stable flow occurs only when the initial flow rate is greater than $\widetilde{\dot{\gamma}}^*$ corresponding to the initial angle μ_n, which is reflected in the jump region of Fig. 1(a). The black, blue, green, red, and pink curves in Fig.3.(a) correspond to S = 0.0, 0.1, 0.2 , 0.4 and 0.6, with the friction coefficient between particles first increasing and then decreasing as pore water content rises, dominated by capillary adhesion below the critical point and lubrication above. Now, let us consider the effects of vibration on these two distinct flow regimes in granular layers. As discussed in Ref.[16], vibration can induce frictional slip at particle contacts, leading to frictional dissipation and reduced shear contact stiffness, thereby decreasing the macroscopic modulus of the granular medium. Additionally, previous studies on single sphere-plane contact configurations have demonstrated that oscillatory sliding reduces the static threshold from μ_s to μ_s^*[13]. This threshold reduction modifies the friction model, as shown in Fig. 3(b), where the reference black solid line for μ_s shifts downward to the black dashed line ($\mu_s^* < \mu_s$). Consequently, whenever the system is loaded, vibration triggers avalanches when $\mu > \mu_s^*$ Specifically, we propose the following scenarios for two distinct applied shear forces: (i) near-threshold shear ($\mu = \mu_1$), satisfying $\mu\left(\widetilde{\dot{\gamma}}_0\right) < \mu_1 \leq \mu_s$, and (ii) sub-threshold shear $\mu = \mu_2 < \mu_d$. For $\mu_1 \leq \mu_s$, flow initiates from a metastable state and persists after vibration ceases, as the system reverts to its initial state (black solid line). The system is driven into the inertial flow regime (III), governed by the term $[\beta_0 + \beta_1\eta(S)]\,\widetilde{\dot{\gamma}}^2$ in Eq. (1). In contrast, for $\mu_2 < \mu_d$ (minimum in the black solid line), the granular system halts flow without vibration and returns to the initial jammed state (I) at $\widetilde{\dot{\gamma}}_0 = 0$. Notably, systems with low pore water saturation (S) exhibit greater vibration-induced lubrication (larger friction reduction), though their initial friction coefficients are higher. As previously noted, in confined granular materials, vibration reduces shear contact stiffness via micro-slip at particle contacts, inducing frictional dissipation and material softening[16][17][18].According to the Mindlin friction model, the reduction in shear contact stiffness $\Delta k_t/k_t$[16] and interparticle friction coefficient $\Delta\mu_p/\mu_p$[13] scales with $-f_t/(\mu_p f_n)$, where f_t is the oscillatory tangential force and f_n is the static normal force per contact. This scaling $(-F_{ac}/(\mu_p W))$ extends to effective shear contact stiffness at multi-contact interfaces[19], shear modulus[17] and yield stress[20] in vibrated granular media, where polydisperse contact roughness is replaced by particle contacts and inertial effects are negligible. Here, F_{ac} is the macroscopic oscillatory shear force, W is the normal load, and μ is the (average) effective interparticle friction coefficient. Thus, we adopt this scaling to describe the reduction in $\Delta\mu_p/\mu_p \sim -F_{ac}/(\mu_p W)$, implying $\mu_s^*/\mu_s \sim 1 - F_{ac}/(\mu_s W)$. For the granular layer, the shear vibration force is expressed as $F_{ac} = \hat{k}\hat{U}$, where $\hat{k}$ is the effective stiffness of the

layer, and $\hat{U}$ is the average displacement amplitude over the layer thickness $h\,(=6\ mm)$. To estimate $\hat{U}$, we assume the amplitude at distance z from the vibration table follows $U(z)\sim U_0\exp(-z/\delta)$, where U_0 is the source amplitude and $\delta\,(\sim\lambda=c/f)$ is the attenuation length dominated by wave scattering[2].

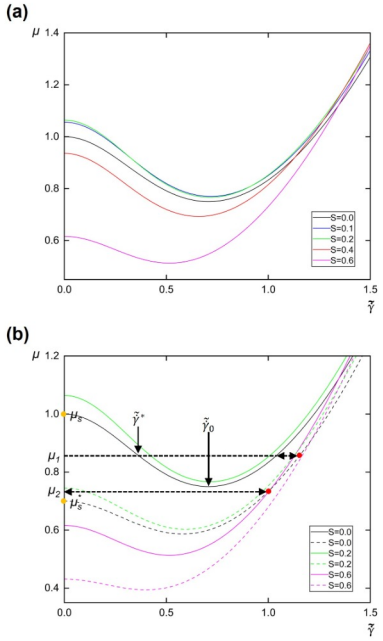

Fig. 3: (a) The effective friction coefficient μ versus flow velocity $\widetilde{\dot{\gamma}}$, as described by Eq. (1) (black solid line), illustrating velocity-weakening behavior for $0<\widetilde{\dot{\gamma}}<\widetilde{\dot{\gamma}}_0$. The minimum shear occurs at $\widetilde{\dot{\gamma}}_0=0.7$, where $\mu_d=0.75$. As pore water saturation increases, the interparticle friction coefficient first rises, then declines beyond a critical saturation. (b)Vibration reduces the interparticle friction coefficient, lowering the yield threshold from $\mu_s=1$ (black solid line) to $\mu_s=0.7$ (black dashed line). The yield criticality also decreases for different pore water content conditions (solid line before applying vibration, dashed line after applying vibration), which triggers the particle flow explained in this paper (red dots).

Thus $\widehat{U}=(1/h)\int_0^h U_0\exp(-z/\delta)dz=(\delta/h)U_0[1-\exp(-h/\delta)]$. In experiments, $\delta\ll h$, so $\hat{U}\sim(\delta/h)U_0\sim(c/fh)U_0$[1]. Using $W\sim(\rho gh)L^2$ and wave speed $c=(G/\rho)^{1/2}$, and introducing a water-dependent attenuation factor $\left[\frac{1}{1+\alpha_2 S^m}\right]$ to account for nonlinear liquid effects, we derive:

$$\frac{\mu_s^*}{\mu_s(S)}\sim 1-\frac{c^3}{g}\cdot\frac{U_0}{\mu_s(S)fh^3}\cdot\left[\frac{1}{1+\alpha_2 S^m}\right] \quad (3)$$

Eq. (3) captures key dependencies, enabling rescaling of experimental data for varying layer thicknesses, pore water saturations, vibration amplitudes, and frequencies (Fig. 2(b)). This scaling aligns with observations in Fig. 2(a), where larger U_0 is required to unjam systems with $S<S_c$. However, residual data scatter after rescaling highlights the need for further studies to quantify layer thickness and frequency effects, improving understanding of transitions between jammed (I) and unjammed (II/III) states.

Conclusion

In summary, we investigated vibration-triggered granular flow under varying wettability. Near the repose angle, reduced μ_p lowers particle threshold μ_s, the mean velocity of the triggered flow increases with vibration amplitude, and this peristaltic flow can only be sustained under prolonged excitation of the vibration and stagnates under excitation shutdown. Near the maximum avalanche angle (θ_m), rapid inertial avalanches occur, dominated by self-driven dynamics. Meanwhile the particle threshold μ_s first rises with the increase of particle pore water content and then rapidly decreases after exceeding the critical water content. We believe that this work provides a unified framework for understanding the behaviour of vibration-triggered granular material flow. Multiscale analyses will contribute to a better understanding of local and remote dynamic triggering of landslides and earthquakes by seismic waves (including aftershocks)[5][21].

References

[1] J. Léopoldès et al. "Triggering granular avalanches with ultrasound". In: *Physical Review E* 102.4 (2020), p. 042901.

[2] X. Jia, C. Caroli, and B. Velicky. "Ultrasound propagation in externally stressed granular media". In: *Physical Review Letters* 82.9 (1999), p. 1863.

[3] C.-h. Liu and S. R. Nagel. "Sound in sand". In: *Physical review letters* 68.15 (1992), p. 2301.

[4] V. Durand et al. "On the link between external forcings and slope instabilities in the Piton de la Fournaise Summit Crater, Reunion Island". In: *Journal of Geophysical Research: Earth Surface* 123.10 (2018), pp. 2422–2442.

[5] C. H. Scholz. *The mechanics of earthquakes and faulting*. Cambridge university press, 2019.

[6] H. A. Makse et al. "Granular packings: Nonlinear elasticity, sound propagation, and collective relaxation dynamics". In: *Physical Review E-Statistical, Nonlinear, and Soft Matter Physics* 70.6 (2004), p. 061302.

[7] E. T. Owens and K. E. Daniels. "Sound propagation and force chains in granular materials". In: *Europhysics Letters* 94.5 (2011), p. 54005.

[8] P. A. Johnson and X. Jia. "Nonlinear dynamics, granular media and dynamic earthquake triggering". In: *Nature* 437.7060 (2005), pp. 871–874.

[9] J. A. Dijksman et al. "Jamming, yielding, and rheology of weakly vibrated granular media". In: *Physical review letters* 107.10 (2011), p. 108303.

[10] A. Daerr and S. Douady. "Two types of avalanche behaviour in granular media". In: *Nature* 399.6733 (1999), pp. 241–243.

[11] P. Coussot et al. "Avalanche behavior in yield stress fluids". In: *Physical review letters* 88.17 (2002), p. 175501.

[12] M. Wyart. "On the dependence of the avalanche angle on the granular layer thickness". In: *Europhysics Letters* 85.2 (2009), p. 24003.

[13] J. Léopoldès, G. Conrad, and X. Jia. "Onset of sliding in amorphous films triggered by high-frequency oscillatory shear". In: *Physical Review Letters* 110.24 (2013), p. 248301.

[14] A. H. Clark et al. "Frictional weakening of vibrated granular flows". In: *Physical Review Letters* 130.11 (2023), p. 118201.

[15] H. Jaeger et al. "Friction in granular flows". In: *Europhysics Letters* 11.7 (1990), p. 619.

[16] X. Jia, T. Brunet, and J. Laurent. "Elastic weakening of a dense granular pack by acoustic fluidization: Slipping, compaction, and aging". In: *Physical Review EStatistical, Nonlinear, and Soft Matter Physics* 84.2 (2011), p. 020301.

[17] J. Brum et al. "Drastic slowdown of the Rayleigh-like wave in unjammed granular suspensions". In: *Physical Review E* 99.4 (2019), p. 042902.

[18] S. Van den Wildenberg, M. van Hecke, and X. Jia. "Evolution of granular packings by nonlinear acoustic waves". In: *Europhysics Letters* 101.1 (2013), p. 14004.

[19] L. Bureau, C. Caroli, and T. Baumberger. "Elasticity and onset of frictional dissipation at a non–sliding multi–contact interface". In: *Proceedings of the Royal Society of London. Series A: Mathematical, Physical and Engineering Sciences* 459.2039 (2003), pp. 2787–2805.

[20] S. van den Wildenberg et al. "Ultrasonic tracking of a sinking ball in a vibrated dense granular suspension". In: *Scientific Reports* 9.1 (2019), p. 5460.

[21] R. Burridge and L. Knopoff. "Model and theoretical seismicity". In: *Bulletin of the seismological society of america* 57.3 (1967), pp. 341–371.